First-principles study of the structural, elastic, and electronic properties of C_{20}, $C_{12}B_8$, and $C_{12}N_8$

2010 J. Phys.: Condens. Matter 22 175505

(http://iopscience.iop.org/0953-8984/22/17/175505)

J. Phys.: Condens. Matter **22** (2010) 175505 (7pp) doi:10.1088/0953-8984/22/17/175505

First-principles study of the structural, elastic, and electronic properties of C_{20}, $C_{12}B_8$, and $C_{12}N_8$

Hong Bin Xu[1], Yuan Xu Wang[1,2,3] and V C Lo[2]

[1] Institute for Computational Materials Science and Physics Department, Henan University, Kaifeng 475004, People's Republic of China
[2] Department of Applied Physics, The Hong Kong Polytechnic University, Hong Kong, People's Republic of China

E-mail: wangyx@henu.edu.cn

Received 30 December 2009, in final form 18 March 2010
Published 12 April 2010
Online at stacks.iop.org/JPhysCM/22/175505

Abstract

First-principles calculations were performed to study the structural, elastic, and electronic properties of the crystalline form of C_{20}, $C_{12}B_8$, and $C_{12}N_8$. These compounds exhibit very different elastic and electronic properties. The shear modulus of $C_{12}N_8$ is much higher than those of C_{20} and $C_{12}B_8$. The strong covalent C–N interaction plays an important role in this high shear modulus. Compared with C_{20}, the relatively small Zener anisotropy of $C_{12}N_8$ is mainly due to its large elastic constant ($C_{11} - C_{12}$). The calculated band structure shows that $C_{12}N_8$ is an insulator with a direct band gap of 3 eV and the other two compounds (C_{20} and $C_{12}B_8$) are metallic. Analysis of the band structure, density of states, and charge density show that the degree of filling in the non-bonding $2p_z$ strongly affects the electronic properties. The full filling of the non-bonding orbital for $C_{12}N_8$ results in its insulating behavior.

(Some figures in this article are in colour only in the electronic version)

1. Introduction

Carbon can form materials in various structures, such as graphite, diamond, C_{60} etc, exhibiting different elastic and electronic properties. Recently, a new hard transparent phase for carbon was found in Russia [1]. Subsequently, Ribeiro *et al* theoretically suggested that this new carbon phase may be simple cubic C_{20} with the $Pm\bar{3}m$ space group [2]. Furthermore, simulation results from molecular dynamics showed that it is dynamically stable up to 1000 K [2].

Unlike diamond, C_{20} crystal is metallic and has relatively small bulk and shear moduli, which are mainly due to the different orbital hybridizations of carbon in C_{20} and diamond. Theoretical analysis shows that there are two kinds of carbon atoms in C_{20}. The atom with the coordination number 4 in the 12j Wyckoff position (12j atom) is sp^3 hybridized, but is very distorted compared to the ideal sp^3 hybridization in diamond. The atom with coordination number 3 in the 8g Wyckoff position (8g atom) is sp^2 hybridized. The 8g atom has a single electron in the $2p_z$ orbital and this single electron is not involved in the hybridization of forming a bond, which yields a higher energy (where z refers to the direction orthogonal to the plane of the sp^2 hybridized orbitals). In addition, the $2p_z$ orbitals of these 8g atoms overlap very weakly. Moreover, the dispersion of the corresponding electronic bands of the 8g atoms is small and their density of states is very sharp. Consequently, the calculated electronic structure shows that C_{20} is metallic [2].

Compared with the half-filled $2p_z$ orbital of the 8g C atom in C_{20}, the $2p_z$ orbital of sp^2 hybridization for the B atom is completely empty and the non-bonding orbital of anisotropic sp^3 hybridization of the N atom is completely filled. Hence, it is desirable when substituting the B and N atoms for the 8g C ones in C_{20} to check the possible improvement of the elastic, stability, and electronic properties. Tian *et al* [3] theoretically found that $C_{12}N_8$ is dynamically stable at ambient pressure and has higher elastic moduli than C_{20}. However, the origin of such improvement for the elastic properties is still unknown. This motivates us to study the electronic structure

[3] Author to whom any correspondence should be addressed.

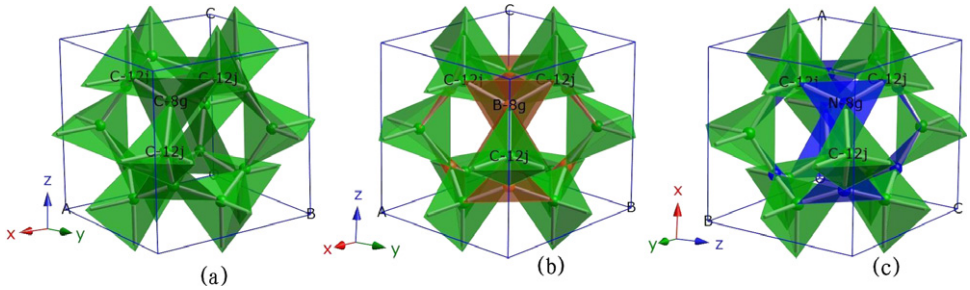

Figure 1. Unit cells of the simple cubic (a) C_{20}, (b) $C_{12}B_8$, and (c) $C_{12}N_8$ with the $Pm\bar{3}m$ space group. The green, brown and blue spheres represent the C, B and N atoms, respectively.

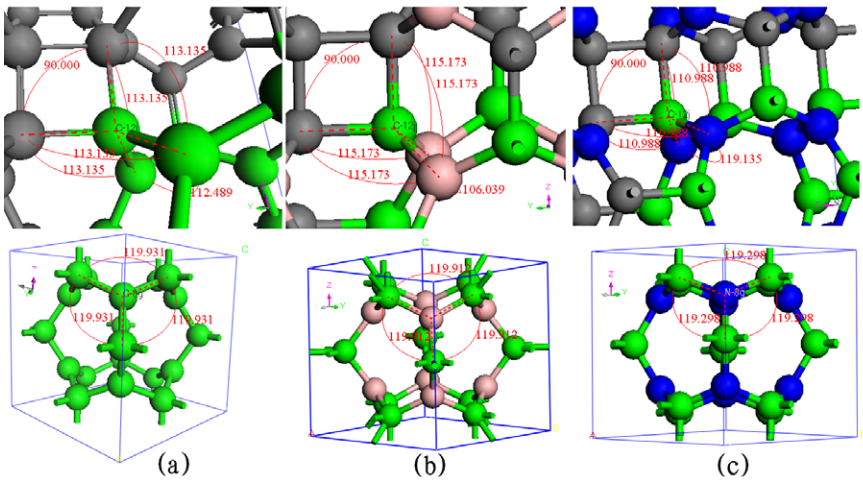

Figure 2. The bond angles in (a) C_{20}, (b) $C_{12}B_8$, (c) $C_{12}N_8$. The angles of the top panels center on the 12j atom and the bottom ones center on the 8g atom.

of the crystalline form of C_{20}, $C_{12}B_8$, and $C_{12}N_8$ to explore the origin of their different elastic properties. Meanwhile, many covalent superhard compounds formed by the light elements B, C, and N have been theoretically studied and experimentally synthesized, such as c-BN, BC_2N, c-BCN, BC_4N etc [4–8]. Their high hardness is always related to their special orbital hybridization and degree of filling into these orbitals.

2. Computational detail

The present calculations were performed within the density functional formalism, using the project-augmented wave (PAW) method [9] facilitated by the Vienna *ab initio* simulation package (VASP) [10, 11]. The PAW potentials used for calculations are constructed by the electron configurations as B $2s^22p^1$, C $2s^22p^2$ and N $2s^22p^3$. The exchange–correlation functional is described by the local density approximation (LDA) [12] and the generalized gradient approximation (GGA) as proposed by Perdew *et al* [13]. The structure was optimized with the conjugate gradient algorithm method and the forces on each ion were converged to less than 0.02 eV $Å^{-1}$. A plane wave cutoff energy of 500 eV was employed throughout. The calculations were performed using a (15, 15, 15) Monkhorst–Pack mesh which corresponds to 120 *k*-points in the irreducible Brillouin zone for all of them.

3. Results and discussions

The optimized structures of C_{20}, $C_{12}B_8$, and $C_{12}N_8$ are shown in figure 1. The unit cells are simple cubic with $Pm\bar{3}m$ symmetry. In each unit cell there are 12 C atoms in the 12j Wyckoff positions and eight C, B, N atoms in the 8g Wyckoff positions of C_{20}, $C_{12}B_8$, $C_{12}N_8$, respectively. Three 12j C atoms elementally form an equilateral triangle, an 8g atom almost lies at the center of gravity. Thus, each 8g atom has three nearest neighbor 12j C atoms to form three nearly two-dimensional σ bonds with three basically identical valence angles close to 120°. Each 12j C atom has two 12j C atoms as nearest neighbors. Furthermore, for C_{20}, $C_{12}B_8$, $C_{12}N_8$, respectively, each 12j atom has two 8g B, C, N atoms to form four three-dimensional σ bonds, in which there is one C–C–C bond with an angle of 90° for all of them. However, the other five bond angles are close to 113° in C_{20}. On the other hand, the B–C–B valence angle in $C_{12}B_8$ is decreased to 106° and its four B–C–C valence angles are slightly increased to 115°. In $C_{12}N_8$, however, the N–C–N valence angle is increased to 119° and its four N–C–C valence angles are decreased to 111°. The valence angles of these compounds are shown in figure 2. The structures of C_{20}, $C_{12}B_8$, and $C_{12}N_8$ can give us an eloquent proof for analyzing the sp^3 and sp^2 hybridization in them.

The calculated lattice constants, Wyckoff positions, and nearest neighbor distances of these compounds are listed in

Table 1. Calculated lattice constants a (in Å), Wyckoff positions (r/a) and nearest neighbor distances d (in Å) for C_{20}, $C_{12}B_8$, and $C_{12}N_8$.

		a	Wyckoff positions	Bond	d
C_{20}	LDA	5.16	C_{12j} (0.500, 0.151, 0.151)	C_{12j}–C_{8g}	1.47
			C_{8g} (0.263, 0.263, 0.263)	C_{12j}–C_{12j}	1.56
	GGA	5.22	C_{12j} (0.500, 0.151, 0.151)	C_{12j}–C_{8g}	1.49
			C_{8g} (0.262, 0.262, 0.262)	C_{12j}–C_{12j}	1.58
$C_{12}B_8$	LDA	5.38	C_{12j} (0.500, 0.146, 0.146)	C_{12j}–B_{8g}	1.56
			B_{8g} (0.269, 0.269, 0.269)	C_{12j}–C_{12j}	1.57
	GGA	5.45	C_{12j} (0.500, 0.146, 0.146)	C_{12j}–B_{8g}	1.57
			B_{8g} (0.268, 0.268, 0.268)	C_{12j}–C_{12j}	1.59
$C_{12}N_8$	LDA	5.03	C_{12j} (0.500, 0.156, 0.156)	C_{12j}–N_{8g}	1.42
			N_{8g} (0.257, 0.257, 0.257)	C_{12j}–C_{12j}	1.57
	GGA	5.09	C_{12j} (0.500, 0.156, 0.156)	C_{12j}–N_{8g}	1.43
			N_{8g} (0.257, 0.257, 0.257)	C_{12j}–C_{12j}	1.59

table 1. From this table, it is found that the C–N bond in $C_{12}N_8$ is shorter and the C–B bond in $C_{12}B_8$ is longer than the corresponding C–C bond in C_{20}. The C–C bond length among 12j atoms has little difference among all these structures. It can be also seen that our calculated results for C_{20} are in excellent agreement with those in [2].

Table 2 lists the calculated equilibrium cell volume, bulk modulus, and pressure derivatives of the bulk moduli of C_{20}, $C_{12}B_8$, and $C_{12}N_8$. The bulk modulus and its pressure derivatives are obtained by fitting the calculated pressure–volume data points to the third-order Birch–Murnaghan equation of state [14]. Compared with C_{20}, the volume of $C_{12}N_8$ contracts (7.1% for LDA and 7.0% for GGA) and that of $C_{12}B_8$ expands (13.6% for LDA and 13.8% for GGA). The decrease of volume in $C_{12}N_8$ is attributed to the stronger covalent C–N interaction than the corresponding C–B and C–C interactions in $C_{12}B_8$ and C_{20}, respectively. The strong covalent C–N interaction in $C_{12}N_8$ results in its smallest unit cell volume and a high incompressibility. The discrepancy in bulk moduli for C_{20} between our results and the value in [2] may mainly be due to the two different methods for estimating the bulk modulus used. The latter work obtained the bulk modulus by fitting the values of the calculated energies at various volumes to a five-parameter empirical function [15].

In order to investigate the elastic stability of the three compounds, their elastic constants were calculated using the strain–stress method [16] and the results are listed in table 3. All C_{ij} of C_{20}, $C_{12}B_8$, and $C_{12}N_8$ observe the following mechanical stability criteria [17, 18] for cubic crystals:

$$C_{11} - C_{12} > 0, \qquad C_{44} > 0, \qquad C_{11} + 2C_{12} > 0 \quad (1)$$

indicating that all of them are elastically stable.

The bulk and shear moduli in table 3 were estimated by the Voigt–Reuss–Hill (VRH) approximation [19]. As shown in this table, the bulk moduli calculated from this method are consistent with those from the third-order Birch–Murnaghan equation of state. The elastic constants C_{ij}, bulk modulus B, shear modulus G, G/B, Young's modulus E, and Poisson's ratio ν of C_{20} and $C_{12}N_8$ agree well with those in [3]. As seen in table 3, the shear modulus of $C_{12}N_8$ is much higher than that of C_{20}. The high shear modulus of $C_{12}N_8$ is mainly due to its large ($C_{11}-C_{12}$) and C_{44}. The large C_{44} of $C_{12}N_8$ indicates that $C_{12}N_8$ has a strong ability to resist the deformation with respect to a shearing stress applied across the (100) plane in the [010] direction. The high values in bulk, shear, and Young's moduli, but a small Poisson's ratio of $C_{12}N_8$ can be attributed to the presence of the strong directional covalent C–N bonding in it.

Table 2. Theoretical equilibrium volume V (in Å^3), bulk modulus B_0 (in GPa), and its pressure derivative B_1 of C_{20}, $C_{12}B_8$, and $C_{12}N_8$ at zero pressure.

		V	B_0	B_1
C_{20}	LDA	137.4	358	3.41
	GGA	142.0	327	3.69
(*Ab initio*) [2]	LDA	138.2	349	
$C_{12}B_8$	LDA	156.1	263	2.72
	GGA	161.6	251	2.78
$C_{12}N_8$	LDA	127.6	399	3.92
	GGA	132.0	372	3.76

As is well known, the shear modulus represents the resistance to plastic deformation, while the bulk modulus represents the resistance to fracture. A high (low) B/G is associated with ductility (brittleness). Ductile and brittle materials can be separated by the critical value of 1.75 for B/G. As shown in table 3, the value of B/G for $C_{12}N_8$ is only 1.03 (GGA), indicating that it is rather brittle. The relatively large B/G of C_{20} and $C_{12}B_8$ show they are less brittle. The stability of a crystal against shear can be determined by the Poisson's ratio ν. The calculated Poisson's ratio for C_{20}, $C_{12}B_8$, and $C_{12}N_8$ are presented in table 3. As seen in this table, the Poisson's ratio of $C_{12}N_8$ is much smaller than those of C_{20} and $C_{12}B_8$. The smaller Poisson's ratio indicates that $C_{12}N_8$ is more stable against shear than C_{20} and $C_{12}B_8$ and has stronger directional bonding. Poisson's ratio is also associated with the volume change during uniaxial deformation. The value of 0.5 for ν represents that there is no change in volume occurring during elastic deformation. The small value of ν for $C_{12}N_8$ indicates its large volume change during deformation. The stiffness of a crystal can be seen from its Young's modulus. We calculated the Young's modulus of the three compounds and list them in table 3. As seen in this table, the Young's modulus of $C_{12}N_8$ is 837 GPa with GGA, which is almost twice that for the other two compounds. The high Young's modulus indicates that $C_{12}N_8$ is relatively stiff. The relative directionality of the bonding in a material has an important effect on its hardness and can be determined by the value of G/B. The calculated G/B for $C_{12}N_8$ is much higher than that for the other two materials. This means that there exists strong directional covalent bonding in $C_{12}N_8$, resulting in its high hardness.

The elastic anisotropy of materials has an important effect on the following phenomena: phase transformation, dislocation dynamics, and other geophysical applications. Zener has introduced an anisotropy index for the cubic crystals by the following expression: $A_Z = \frac{2C_{44}}{C_{11}-C_{12}}$ [20]. When $A_Z = 1$, it is restored to the isotropic condition. The calculated A_Z for $C_{12}N_8$ is 0.89 (GGA) which is less than the 1.76 for C_{20}. As shown in table 3, by comparison with C_{20}, the relatively small Zener anisotropy of $C_{12}N_8$ is mainly due to its large

Table 3. Calculated elastic constants C_{ij} (in GPa), bulk modulus B (in GPa), shear modulus G (in GPa), B/G, G/B, Young's modulus E (in GPa), and Poisson's ratio ν of C_{20}, $C_{12}B_8$, and $C_{12}N_8$.

		C_{11}	C_{12}	C_{44}	B	G_V	G_R	G_H	B/G	G/B	E	ν
C_{20}	LDA	577	296	259	389	212	240	226	1.72	0.58	568	0.26
	GGA	527	230	262	329	216	247	231	1.43	0.70	562	0.22
	LDA [3]	550	245	256	347			153	2.27	0.44	400	0.31
	GGA [3]	561	227	272	338			167	2.04	0.49	430	0.29
$C_{12}B_8$	LDA	345	217	177	260	132	129	131	2.00	0.50	336	0.28
	GGA	350	190	178	243	139	148	143	1.69	0.59	359	0.25
$C_{12}N_8$	LDA	901	160	332	407	348	418	383	1.06	0.94	875	0.14
	GGA	862	142	319	382	336	403	369	1.03	0.97	837	0.14
	LDA [3]	880	149	327	393			366	1.08	0.93	838	0.15
	GGA [3]	867	137	327	380			365	1.04	0.96	829	0.14

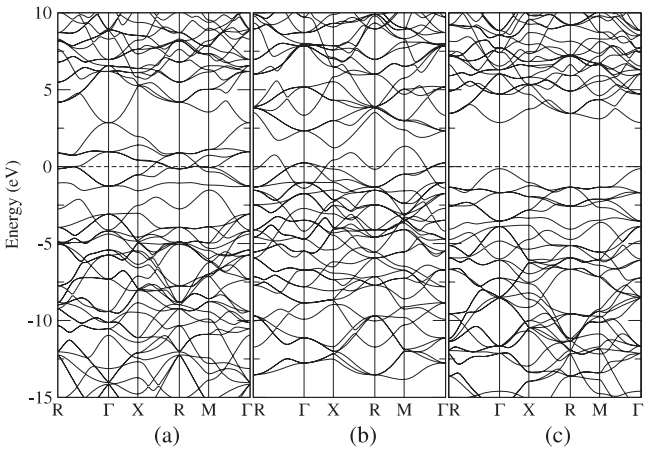

Figure 3. Calculated electronic band structure of (a) C_{20}, (b) $C_{12}B_8$, and (c) $C_{12}N_8$ at zero pressure. The high symmetry k points R, Γ, X, and M represent the points (1/2, 1/2, 1/2), (0, 0, 0), (1/2, 0, 0), and (1/2, 1/2, 0), respectively.

$(C_{11} - C_{12})$. Because of this large difference in A_Z, it is necessary to check the difference in their upper and lower limits for the corresponding shear modulus. The Reuss shear modulus (G_R) [21] and the Voigt shear modulus (G_V) [22] represent the upper and lower limits of the shear modulus, respectively. As shown in table 3, compared with C_{20}, both the upper and lower limits of the shear modulus dramatically increase. In particular, the value of G_V for $C_{12}N_8$ is larger than those of G_R for C_{20} and $C_{12}B_8$. This means that the lower limit of the shear modulus for $C_{12}N_8$ is larger than the upper limits of the shear modulus for C_{20} and $C_{12}B_8$. Moreover, compared with C_{20}, the dramatic change of G_R for $C_{12}N_8$ causes an increment of the difference between their shear moduli and Young's moduli.

In order to unveil the different elastic behaviors for C_{20}, $C_{12}B_8$, and $C_{12}N_8$, their electronic structures were calculated. Figure 3 shows their band structures under the LDA. From this figure, C_{20} is metallic. An analysis of the orbital hybridization is helpful for understanding the metallic behavior of C_{20}. For the 8g C atom, one of the paired 2s electrons gets promoted to the 2p orbital, so there are three unpaired electrons respectively occupying the $2p_x$, $2p_y$, and $2p_z$ orbitals. Upon forming a bond, the 2s orbital is mixed with only two of the three available 2p orbitals to form three sp^2-hybrid orbitals. The three sp^2-hybrid orbitals are arranged in the same plane, making an angle of 120° with each other. Each sp^2 hybrid orbital overlaps with a sp^3 hybrid orbital of the 12j C atom and the six valence electrons (three from 8g C and the other three from 12j C) form three two-dimensional σ-bonds. However, the $2p_z$ orbital oriented along the axis perpendicular to the hybridization plane is half-filled and is not involved in hybridization to form a bond. Consequently, the energy of the half-filled and non-bonding $2p_z$ orbital is higher than the Fermi energy.

Compared with the metallic behavior in C_{20}, $C_{12}N_8$ is an insulator with a large direct band gap of 3 eV. The true band gap should be larger than this calculated value since the LDA always underestimates band gap. Both the top of the valence bands and the bottom of the conduction bands of $C_{12}N_8$ are located at the Γ point. Since the valence electron configuration of the N atom is $2s^22p^3$, each 2p orbital is already occupied by one electron. As one of two paired 2s electrons is excited to the $2p_z$ orbital, it is coupled to the $2p_z$ electron. Consequently, one of the four sp^3-like hybridized orbitals in the N atom is fully filled and does not form bonds with other atoms. The two $2p_z$ non-bonding electrons are frequently called the lone electron pair. The other three sp^3-like hybrid orbitals form three normal σ-bonds with the 12j C atoms. Thus, the full filling of the non-bonding $2p_z$ orbital causes the insulating property in $C_{12}N_8$ and lowers the total energy. The presence of the lone pair electrons in the N atom has an important effect on its various properties.

As for the behavior of the orbital hybridization for $C_{12}B_8$, figure 3 reveals that $C_{12}B_8$ is metallic. The valence electron configuration of the B atom is $2s^22p^1$. Thus, when one of the two paired 2s electrons is promoted to the $2p_y$ orbital, the $2p_z$ orbital remains empty. In the sp^2 hybridization, the 2s, $2p_x$, and $2p_y$ orbitals of the B atom are mixed into three hybridized orbitals and form three σ-bonds with the 12j C atoms. The empty $2p_z$ orbital, which is not involved in the sp^2-hybridization, is perpendicular to the plane of the hybridized orbitals. The unoccupied $2p_z$ orbital can also be observed from the band structure. As shown in figure 3, the shape of the band structure of $C_{12}B_8$ is very similar to C_{20} except for their different Fermi energy levels. Compared with the lower energy bands of the half-filled $2p_z$ orbital in C_{20}, the corresponding bands in $C_{12}B_8$ shift above the Fermi energy and become empty bands. Another difference in band structure between $C_{12}B_8$ and C_{20} is the existence of a flat band around

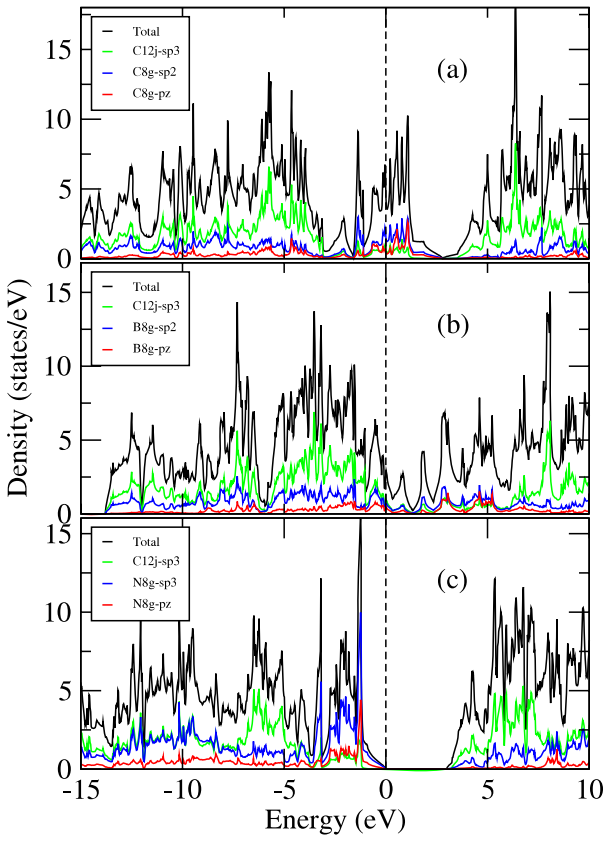

Figure 4. Calculated density of states of (a) C_{20}, (b) $C_{12}B_8$, and (c) $C_{12}N_8$. The sp^3 (2s, $2p_x$, $2p_y$, $2p_z$) PDOS of C in the 12j Wyckoff positions, the sp^2 (2s, $2p_x$, $2p_y$), p_z PDOS of C, B in C_{20} and $C_{12}B_8$, and the sp^3, p_z PDOS of N in $C_{12}N_8$ are given too.

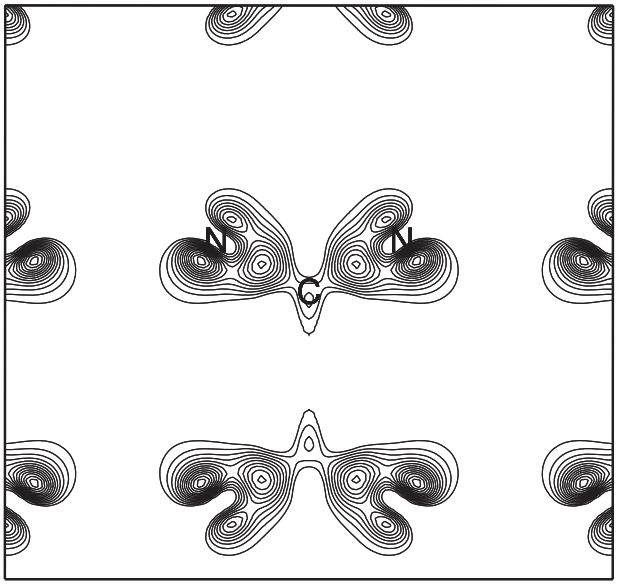

Figure 5. The difference charge density contour plot for $C_{12}N_8$ in the plane containing the 12j C atom and two nearest neighbor 8g N atoms. The values of the contours in this figure are from 0 to 1 e Å^{-3} with an increment of 0.05 e Å^{-3}.

−2 eV in C_{20}. This flat band is mainly due to the sp^2 hybrid orbital of the 8g C atoms and partially to the sp^3 hybrid orbital of the 12j C atoms (as shown in figure 4). Moreover, this flat

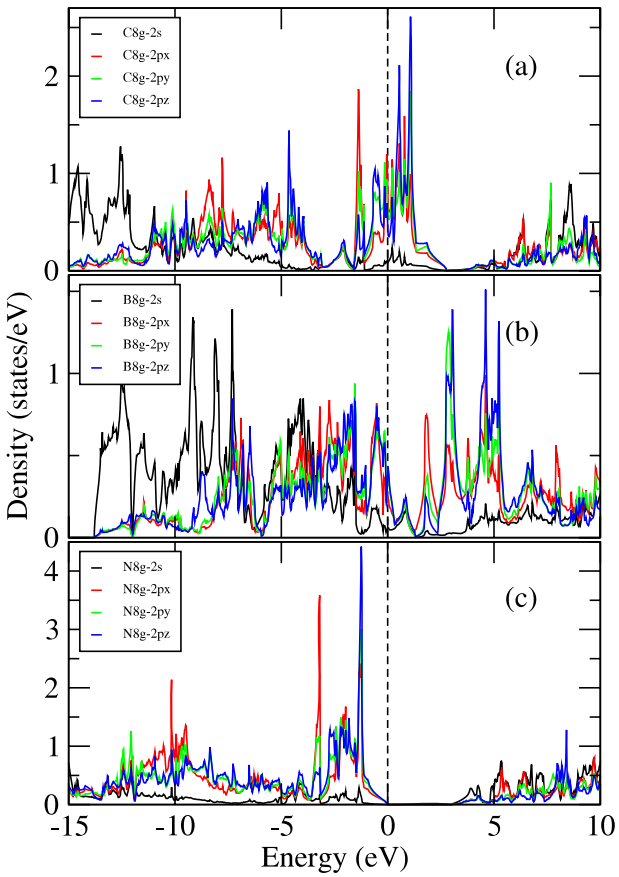

Figure 6. The 2s, $2p_x$, $2p_y$, and $2p_z$ PDOS of the C, B, and N atoms in the 8g Wyckoff positions for (a) C_{20}, (b) $C_{12}B_8$, and (c) $C_{12}N_8$, respectively.

band slightly overlaps with other bands, indicating its localized character. It is interesting that the energy band profile of $C_{12}B_8$ is very similar to that of boron-doped diamond except for the different position of the top of the valence band [23].

The calculated densities of states (DOS) for C_{20}, $C_{12}B_8$, and $C_{12}N_8$ are shown in figure 4. It can be clearly seen that the total DOS at the Fermi level is higher for C_{20}. The half-filled $2p_z$ orbital of the 8g C atoms induces its metallic behavior. The states on the Fermi level drop quickly for $C_{12}B_8$ and disappear for $C_{12}N_8$, indicating that incorporating eight B and N atoms in the C_{20} unit has rather unsurprisingly a major influence on the underlying electronic structure, due to the disruption of the π and/or σ conjugation. $C_{12}N_8$ is the most stable, and is a semiconductor. As seen in figure 4, the shape of the partial density states (PDOS) of the 12j C atoms is very similar to that of the 8g atoms, indicating a strong orbital hybridization between the 12j and 8g atoms. In particular, in the energy range of −15 to −8 eV for $C_{12}N_8$, the shape and height of the sp^3 PDOS of the 12j C atoms are very close to those of the sp^3 PDOS of the 8g N atoms. This implies a strong covalent interaction between the C and N atoms. This strong C–N covalent interaction is the cause of the shorter length and high strength of the C–N bond. Consequently, $C_{12}N_8$ has a higher resistance to both elastic and plastic deformation. The strong covalent C–N interaction is also evidenced by the difference charge density of $C_{12}N_8$ shown in figure 5.

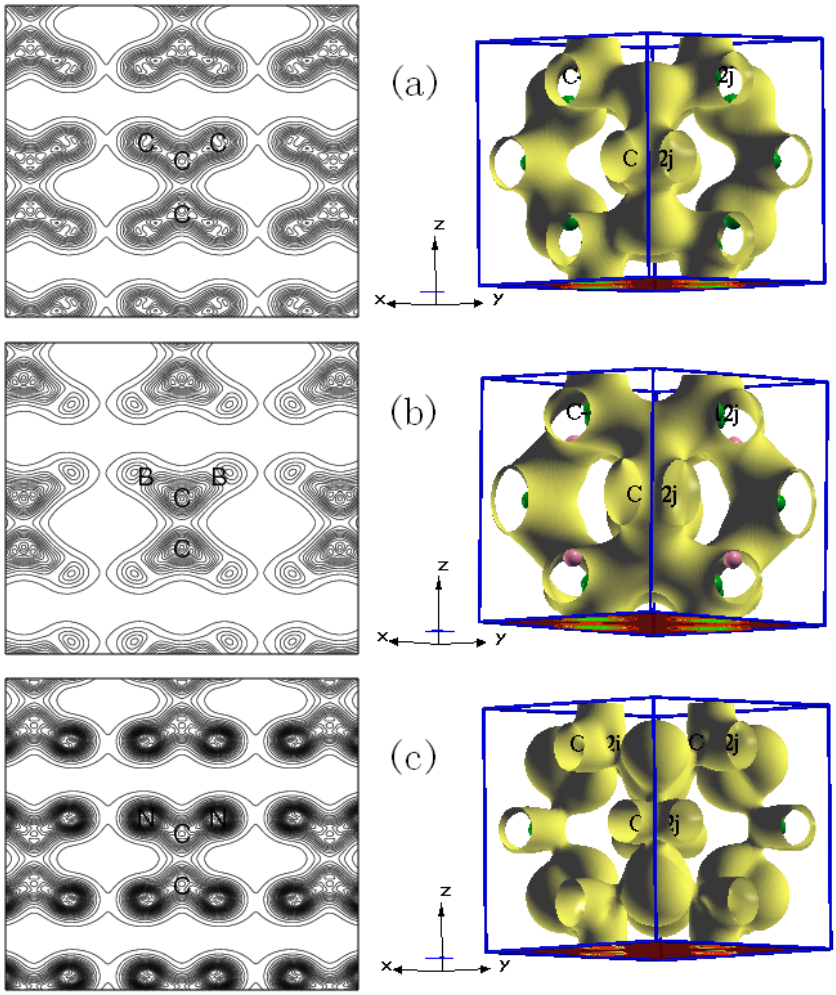

Figure 7. Calculated occupied charge density in the energy range of −6–0 eV of (a) C_{20}, (b) $C_{12}B_8$, and (c) $C_{12}N_8$. The left panels are plotted with an increment of 0.15 e Å^{-3}. Isosurface plots on the right panels are at a charge density of 0.2 e Å^{-3}.

For further investigation of the properties of bonding orbitals and non-bonding orbitals of the 8g atoms, their 2s, $2p_x$, $2p_y$, and $2p_z$ PDOS are calculated and the results are plotted in figure 6. Obviously, there is always a nearly overlapping part of these curves from −12 to 0 eV, reflecting the strong hybridization between them. The 2s, $2p_x$, $2p_y$, and $2p_z$ PDOS of the 8g atoms can provide useful information for analyzing the sp^2 hybridization of C (B) in C_{20} ($C_{12}B_8$) and sp^3-like hybridization of N in $C_{12}N_8$. As seen in figure 6, compared with the 8g C atoms and the 8g N ones, the main peaks of PDOS for the 8g B atoms shift to the higher energy range, which is partially caused by the empty non-bonding $2p_z$ orbital. For $C_{12}N_8$, the full filling of the non-bonding $2p_z$ orbital results in the shifting of the corresponding PDOSs to the lower energy range. Consequently, the total energy of $C_{12}N_8$ decreases and becomes more stable. Moreover, for $C_{12}N_8$, the PDOS of the $2p_z$ orbital around −2 eV is very sharp, confirming the non-bonding state of the $2p_z$ orbital of the N atoms. Therefore, the degree of filling in the non-bonding $2p_z$ orbital can strongly affect the electronic properties and the stability of these compounds.

The orbital hybridization and the degree of filling in the non-bonding $2p_z$ orbital for the 8g atoms can also be analyzed from their charge density as shown in figure 7. The central axis of three σ-bonding hybrid orbitals of the C, B, and N atoms is parallel to the plane shown in the left panels of figure 7. The central axis of the non-bonding orbitals is perpendicular to the plane mentioned above. As shown in figure 7, the difference in charge density along the non-bonding direction is particularly noticeable for C, B, and N. The charge density of the non-bonding orbital for the 8g N atoms is much higher than those for the 8g B atoms and the 8g C ones. The charge density of the 8g B atoms is the lowest because of its unoccupied non-bonding $2p_z$ orbital. The difference in charge density for the bonding orbitals of the three compounds is very small. Therefore, the charge density distribution shown in figure 7 clearly demonstrates orbital hybridization and the degree of filling in the non-bonding orbital for the 8g atoms in these compounds.

4. Conclusion

In summary, we have investigated the structural, elastic, and electronic properties of the crystalline form of C_{20}, $C_{12}B_8$, and $C_{12}N_8$. The shear modulus of $C_{12}N_8$ is much higher those of

C_{20} and $C_{12}N_8$. The high shear modulus of $C_{12}N_8$ is mainly due to its strong covalent C–N interaction. The structure, density of states, and charge density for C_{20}, $C_{12}B_8$, and $C_{12}N_8$ show a clear image of three σ-bonding hybridized orbitals and the degree of occupation for the non-bonding orbitals which are not involved in hybridization for the 8g atoms. The fully filled non-bonding orbital for $C_{12}N_8$ results in its insulating behavior and partially contributes to the strong covalent interaction between the C and N atoms. Consequently, it is concluded that the saturation of non-bonding orbital can strongly affect the electronic properties of the three compounds.

Acknowledgments

This research was sponsored by The Hong Kong Polytechnic University through University Research Grant no. 1-ZV44, the Program for Science&Technology Innovation Talents in Universities of Henan Province (no. 2009HASTIT003), the Foundation of Science and Technology Department of Henan Province (no. 082300410010).

References

[1] El Goresy A, Dubrovinsky L S, Gillet P, Mostefaoui S, Graup G, Drakopoulos M, Simionovici S, Swamy V and Masaitis V 2003 *C. R. Geosci.* **335** 889
[2] Ribeiro F J, Tangney P, Louie S G and Cohen L 2006 *Phys. Rev.* B **74** 172101
[3] Tian F, Wang J, He Z, Ma Y, Wang L, Cui T, Chen C, Liu B and Zou G 2008 *Phys. Rev.* B **78** 235431
[4] Zhang Y, Sun H and Chen C 2005 *Phys. Rev. Lett.* **94** 145505
[5] Pan Z, Sun H and Chen C 2007 *Phys. Rev. Lett.* **98** 135505
[6] Chen S and Gong X G 2007 *Phys. Rev. Lett.* **98** 015502
[7] Yuge K, Seko A, Koyama Y, Oba F and Tanaka I 2008 *Phys. Rev.* B **77** 094121
[8] Chen S and Gong X G 2008 *Phys. Rev.* B **77** 014113
[9] Blochl P E 1994 *Phys. Rev.* B **50** 17953
[10] Kresse G and Furthmuller J 1996 *Comput. Mater. Sci.* **6** 15
[11] Kresse G and Furthmuller J 1996 *Phys. Rev.* B **54** 11169
[12] Ceperley D M and Alder B J 1980 *Phys. Rev. Lett.* **45** 566
[13] Perdew J P, Burke K and Ernzerhof M 1996 *Phys. Rev. Lett.* **77** 3865
[14] Birch F 1947 *Phys. Rev.* **71** 809
[15] Ribeiro F J, Tangney P, Louie S G and Cohen M L 2005 *Phys. Rev.* B **72** 214109
[16] Wang Y X 2007 *Appl. Phys. Lett.* **91** 101904
[17] Born M and Huang K 1956 *Dynamical Theory of Crystal Lattices* (Oxford: Clarendon)
[18] Nye J F 1985 *Physical Properties of Crystal* (Oxford: Oxford University Press)
[19] Hill R 1952 *Proc. Phys. Soc. Lond.* **65** 349
[20] Zener C 1948 *Elasticity and Anelasticity of Metals* (Chicago, IL: University of Chicago Press)
[21] Reuss A 1929 *Z. Angew. Math. Mech.* **9** 55
[22] Voigt W 1928 *Lehrbuch der Kristallphsik* (Leipzig: Taubner)
[23] Lee K-W and Pickett W E 2004 *Phys. Rev. Lett.* **93** 237003